AAPS PharmSciTech, Vol. 19, No. 8, November 2018 (© 2018)
DOI: 10.1208/s12249-018-1147-4

Research Article

Theme: Lipid-Based Drug Delivery Strategies for Oral Drug Delivery
Guest Editor: Sanyog Jain

Novel Self-Assembled Ibrutinib-Phospholipid Complex for Potently Peroral Delivery of Poorly Soluble Drugs with pH-Dependent Solubility

Qiujun Qiu,[1] Mei Lu,[1] Cong Li,[1] Xiang Luo,[1] Xinrong Liu,[1] Ling Hu,[1] Mingqi Liu,[1] Huangliang Zheng,[1] Hongxia Zhang,[1] Min Liu,[1] Chaoyang Lai,[1] Yanzhi Song,[1,2] and Yihui Deng[1,2]

Received 8 June 2018; accepted 8 August 2018; published online 12 September 2018

Abstract. As an irreversible small-molecule kinase inhibitor, ibrutinib (IBR) exhibits excellent tumor suppression in various tumor cells. However, IBR is insoluble at neutral pH and can dissolve only at low pH: thus, commercial IBR products present poor bioavailability and weakened *in vivo* antitumor activity. Therefore, we aimed to develop a stable IBR-phospholipid complex (IBR-PC) using egg phosphatidylglycerol (EPG) as excipients to improve the bioavailability of IBR and further enhance its antitumor effects. IBR-PC was characterized by transmission electron microscopy (TEM), Fourier transform infrared spectroscopy (FT-IR), differential scanning calorimetry (DSC), X-ray powder diffraction (XPRD), and molecular docking and simulation test, which all explained the interactions of two components. Solubility tests demonstrate that the novel formulation can maintain excellent solubility (above 5 mg/mL) at various pH levels. Storage stability tests show that no change in particle size or content of IBR-PC was observed during the experimental period. *In vivo* pharmacokinetic results demonstrated that the relative bioavailability of IBR-PC was a 9.14-fold improvement relative to that of IBR suspension (IBR-susp). Furthermore, IBR-PC was associated with enhanced cytotoxic activity *in vitro* and superior tumor growth suppression *in vivo* compared to that resulting from the free IBR. Thus, the proposed IBR-PC system is a promising drug delivery system that enhances the oral bioavailability of IBR, resulting in its improved *in vivo* antitumor effect.

KEY WORDS: ibrutinib; phospholipid complex; egg phosphatidylglycerol; bioavailability; antitumor activity.

INTRODUCTION

With the elucidation of tumor pathogenesis and signaling pathways, kinase inhibitors have been widely used to treat cancer. Ibrutinib (IBR) is an orally administered, irreversible, and potent inhibitor of Bruton's tyrosine kinase, and it is recognized by the FDA as a breakthrough therapy and orphan drug designation for the treatment of several malignant tumors, including chronic lymphocytic leukemia and chronic graft-*versus*-host disease (1–5). IBR's R&D is a landmark discovery that has made the treatment of many malignant diseases possible. In addition, IBR has been heavily reported to efficiently block the activation of several other kinases such as ITK, TEC, JAK3, HCK, BLK, and especially ERBB receptor family, indicating that IBR can be exploited for the treatment of multiple tumors in the future (6–10). Several clinical trials currently evaluate the efficacy of IBR against metastatic pancreatic adenocarcinoma (NCT02436668), cutaneous melanoma (NCT02581930), and EGFR mutation-positive non-small cell lung cancers (NCT02321540) (2).

However, IBR is soluble at low pH values but nearly insoluble at neutral pH values, which lead to low bioavailability and impede its *in vivo* antitumor effect after oral administration (11). In fact, the oral bioavailability of IBR is only approximately 3% (12). Given its extremely low absorption efficiency, high doses of IBR are required to ensure efficacy. IBR is produced in the form of capsules (140 mg per capsule), and the highest dosage used in mantle cell lymphoma treatment is 560 mg per day. Furthermore, the increased pH probably causes the drug to precipitate when IBR is transported from the stomach to the intestine (6). High drug doses and intestinal precipitation lead to a series of severe gastrointestinal side effects, including diarrhea and nausea (13).

Qiujun Qiu and Mei Lu contributed equally to this work.

Guest Editor: Sanyog Jain

[1] College of Pharmacy, Shenyang Pharmaceutical University, 103 Wenhua Road, Shenyang, 110016, Liaoning, China.
[2] To whom correspondence should be addressed. (e-mail: songyanzhi@syphu.edu.cn; dengyihui@syphu.edu.cn)

Crystalline changes, solid dispersion technology, acid addition salt, and self-assembled nanoemulsion reportedly promote the water solubility and bioavailability of IBR (12,14–17). However, serious drawbacks have been noted in the current formulation technologies, including insignificant increase in solubility and over-reliance of drug dissolution on pH, resulting in failure to effectively increase the bioavailability of IBR. The decreased daily dosage can reduce the risk of side effects, but this approach requires a new formulation to improved utility of IBR.

Since the initial synthesis of pharmaceutical phospholipid complex (PC) in 1989 in Italy, drug-PC has been extensively investigated as efficient drug delivery carriers for enhancing the solubility and bioavailability of several poorly soluble drugs (18–20). This technique involves the formation of a complex between phospholipid molecules containing polar groups and specific active pharmaceutical components *via* hydrogen bonding, thereby enhancing the solubility, membrane permeability, and ultimately the systemic bioavailability of the drugs (21,22). Furthermore, drug-PC is increasingly resistant to changes in pH and gastrointestinal motility and further decreases gastrointestinal toxicity (23). Although many phospholipids have been utilized for the preparation of PC, this is the first ever attempt to report egg phosphatidylglycerol (EPG) as an excipient. The special structure of EPG makes it more hydrophilic and easier to self-assemble. Thus, preparation of ibrutinib-phospholipid complex (IBR-PC) with EPG is a worthy attempt.

The objective of the present study was to develop a novel ibrutinib-phospholipid complex (IBR-PC) delivery system for promotion the absorption of IBR and enhancement of patient compliance. *In vitro* solubility tests and dissolution test involving simulated gastrointestinal fluid (SGIF) were performed to demonstrate the increased solubility and dissolution behavior of IBR-PC. *In vitro* cytotoxicity test was performed to illustrate the enhanced toxicity of IBR-PC. Moreover, an *in vivo* pharmacokinetic study in rats was performed to confirm the observed increased drug absorption and improved bioavailability. Finally, an exhaustive analysis of the enhanced tumor inhibition in tumor-bearing mice was performed. The present results reveal that the self-assembled IBR-PC system is a prospective drug delivery system for enhancing the bioavailability and antitumor effect of IBR.

MATERIALS AND METHODS

Materials

Materials are listed as follows:

IBR (purity > 99%) was purchased from Nanjing Xize Biotechnology Co., Ltd. (Jiangsu, China). EPG was purchased from Shanghai Advanced Vehicle Technology Co., Ltd. (Shanghai, China). Egg phosphatidylcholine (E80), soy lecithin (S100), and dioleoylphosphatidic acid (DOPA) were purchased from LIPOID GmbH Co. (Ludwigshafen, Germany). Phosphatidylserine (PS90) was purchased from Beijing Bewell Pharmaceutical Technology Co., Ltd. (Beijing, China). Tolbutamide (purity > 99%) was purchased from Dalian Meilun Biotechnology Co., Ltd. (Liaoning, China). All chemicals used in this study were of analytical or high-performance liquid chromatography (HPLC) grade.

Cells and Animals

S180 murine sarcoma cell lines were obtained from the Cell Bank of the Chinese Academy of Sciences (Shanghai, China). Male Wistar rats (aged 7–8 weeks weighing 180–220 g) and male Kunming mice (aged 6–7 weeks weighing 18–22 g) were purchased from the Central Animal Laboratory of Shenyang Pharmaceutical University (Liaoning, China). All animal experiments were performed in accordance with the guidelines of the Animal Welfare Committee of Shenyang Pharmaceutical University. The protocol numbers of the animal studies were SYPU-IACUC-C2018-1-24-201 and SYPU-IACUC- C2018-4-4-101.

Preparation of IBR-PC

Given that solvent evaporation is one of the most ubiquitous methods to fabricate PC and both EPG and IBR are easily soluble in ethanol (24), IBR-PC was prepared using the solvent evaporation method. In brief, IBR and different types of phospholipids (EPG, S100, E80, DOPA, and PS90) were dissolved in anhydrous ethanol at defined molar ratios (2:1, 1:1, 1:2, and 1:3). The optimal drug concentration (5, 10, 15, and 20 mg/mL) is based on the highest complexation rate. The mixture was refluxed at different temperatures (30°C, 40°C, 50°C, and 60°C) for a certain period of time (0.25, 0.5, 1, 1.5, and 2 h). Subsequently, ethanol was evaporated at the same temperature to near dryness. The resulting complexes were hydrated with distilled water for 10 min under fast stirring to form the final PC. To remove the insoluble particles, we filtered the suspension through 0.45-μm filter membranes. Sucrose, lactose, or maltose (*lyoprotectant*) was added (5%, *m*/*v*) into the PC to reduce the expansion of particles during freeze-drying. Lyophilized formulations were reconstituted using distilled water under gentle shaking. On the basis of the complexation rate and appearance of IBR-PC, we determined the optimal formulation and processing parameters.

Preparation of IBR Suspension

To obtain an IBR suspension, we dissolved the IBR in distilled water in the presence of croscarmellose sodium. Sodium lauryl sulfate, magnesium stearate, and microcrystalline cellulose were added under stirring to obtain an oral IBR suspension (IBR-susp).

Determination of IBR Content in PC

EPG and PC both dissolved easily in solution medium, but pure IBR remained practically insoluble. Following the method described in the "Preparation of IBR-PC" section, after removal of non-complexed insoluble particles by filtration, the complex solution was diluted with methanol in triplicate to a linear concentration range and then analyzed on a UV-1801 UV/VIS spectrophotometer (Beijing Rayleigh Analytical Instrument Co., Ltd., China) at 260 nm. IBR content of PC can be calculated from standard curves and expressed as mean standard deviation. The standard regression equation in the range of $C = 5.0$ μg/mL to 13.0 μg/mL was linear ($A = 0.0503C + 0.0107$, $r = 0.9999$; A means absence

of IBR). The recoveries are 100.27% ± 0.33%, indicating the reliability of the above method for determination under the described conditions. The complexation rate of IBR in PC was determined as follows:

$$\text{Complexation rate} = \frac{m_2}{m_1} \times 100\%$$

where m_1 is the total content of IBR added and m_2 is the amount of complexed IBR.

Characterization of IBR-PC

Particle Size and Zeta Potential

The mean particle size, polydispersity index (PDI), and zeta potential of IBR-PC were measured by a NICOMP™ 380 Submicron Particle Sizer (CA, USA). All samples were diluted with distilled water, and the experiments were conducted in triplicate at 25°C ± 2°C.

Transmission Electron Microscopy

IBR-PC was stained with phosphotungstic acid solution (2%, *m*/*v*), pipetted on Formvar film-coated copper grids with a mesh size of 200 nm (Beijing Zhongjingkeyi Technology Co., Ltd., China), and dried at room temperature. The morphological evaluation of IBR-PC was performed using a transmission electron microscopy (TEM) (JEM-2100, JEOL Co., Ltd., Japan).

Fourier Transform Infrared Spectroscopy

Fourier transform infrared spectroscopy (FT-IR) spectra of bulk IBR, blank excipients (EPG), IBR/EPG mixture, and IBR-PC were recorded on a spectrometer (Bruker IFS 55, Bruker, Germany) within the *wave number* range of 500–4000 cm^{-1}. A total of 16 scans were obtained at a resolution of 2 cm^{-1}. To prepare the pellets, we mixed the samples with KBr and then compressed them at 10 MPa for 5 min by using a hydraulic press to produce discs with a 10-mm diameter.

Differential Scanning Calorimetry

Thermal properties of bulk IBR, EPG, IBR/EPG mixture, and IBR-PC were analyzed using differential scanning calorimetry (DSC) (DSC1, Mettler Toledo Co., Ltd., Switzerland). The samples were placed in sealed aluminum pans with perforated lids. Measurements were obtained at 30–200°C at a heating rate of 10°C/min. Measurements were performed under nitrogen flow at a rate of 40 mL/min.

X-ray Powder Diffraction

X-ray powder diffraction (XRPD) patterns of bulk IBR, EPG, IBR/EPG mixture, and IBR-PC were obtained using an X-ray diffractometer (DX-2800, Dandong Haoyuan Instrument Co., Ltd., China). XRPD was performed in symmetrical reflection mode using Cu-Kα radiation generated at 40 kV and 30 mA. The sample was placed on a flat aluminum sample holder, and a scanning rate of 2°/min from 5 to 35° at 2θ intervals was used.

Molecular Docking and Simulation Studies

Computer-aided molecular modeling and simulation studies for conformational analysis of the interaction between IBR and EPG during complexation were performed by using AutoDock Vina software, and the MMFF force field was used for this analysis (25).

Solubility Test

The solubility of IBR-susp and IBR-PC in media at different pH values was determined. An excess amount of IBR-susp or IBR-PC was added into 5 mL of each solvent in sealed glass containers. The samples were shaken at 25°C for 24 h and then centrifuged at 10000 rpm for 10 min. The supernatant was filtered through a 0.45-μm membrane and then diluted with methanol for IBR quantification at 260 nm by a UV/VIS spectrophotometer.

In Vitro Dissolution Test in SGIF

Given the effects of pH and gastrointestinal movement on the dissolution of PC in the gastrointestinal tract, an *in vitro* dissolution test of IBR-PC in SGIF was performed using paddle method (according to the Chinese Pharmacopeia 2015) with a dissolution tester (RCZ-6B, Shanghai Huanghai, China) under a rotation speed of 75 rpm to simulate the gastrointestinal movement.

In brief, the formulation was added to simulated gastric fluid (SGF, pH 1.2) at 37°C and then stirred for 2 h. Next, the medium was adjusted to the simulated intestinal fluid (SIF, pH 6.8) by adding 0.2 mol/L Na_3PO_4 solution under continuous stirring for 4 h. At each predetermined time interval (10, 20, 30, 45 60, 120, 130, 140, 150, 165, 180, 240, 300, and 360 min), an aliquot of 5 mL was withdrawn from the medium and replaced by an equal volume of temperature-equilibrated medium. Afterward, the concentration of IBR was determined a UV/VIS spectrophotometer as described above. IBR-susp was used as control.

Long-term Stability of Lyophilized IBR-PC

Long-term stability of lyophilized IBR-PC was determined after storage at 4 ± 2°C for 6 months. After the addition of exactly 5 mL of distilled water, the lyophilized IBR-PC powder reformed a clarified solution under continuous shaking. Particle size and zeta potential were determined after 1, 2, 3, and 6 months as described in the "Particle Size and Zeta Potential" section. IBR-PC content was assayed after the preset period of time elapsed as described in the "Determination of IBR Content in PC" section.

In Vitro Cytotoxicity (MTT) Assay

The *in vitro* cytotoxicity of different IBR formulations was assessed using MTT assay. Briefly, the S180 cells were seeded in 96-well plates and incubated with different IBR formulations at various concentrations for 48 h. After 48 h of

incubation, MTT solution (5 mg mL^{-1}) was added to each well (10 μL), and cells were incubated for an additional 4 h. The reaction was stopped by the addition of 100 μL of dissolving solution and the absorbance was measured at 570 nm using a Microplate reader (Bio-Rad Laboratories Ltd., Hertfordshire, UK). The half maximal inhibitory concentrations (IC_{50}) which can indirectly reflect the cytotoxicity of different IBR formulations were calculated.

In Vivo Pharmacokinetic Studies

Male Wistar rats were randomly divided into two groups of three rats each. These groups were orally administered with 20 mg/kg IBR-susp and IBR-PC, respectively. Blood samples were collected from the orbital sinus at a specific time point (1, 5, 15, and 30 min and 1, 2, 4, 8, 12, and 24 h).

Plasma was isolated from the blood sample by centrifugation at 4500 rpm for 10 min. Afterward, 0.1 mL of 10 μg/mL tolbutamide solution as internal standard was added into each blood sample and then diluted with 0.6 mL of methanol. All blood samples were subjected to centrifugation at 10000 rpm for 10 min. The supernatants were evaporated using a nitrogen stream; the evaporated samples were redissolved with 100 μL of mobile phase and then centrifuged at 10000 rpm for 10 min. The concentrations of IBR in the supernatants were measured using HPLC. The standard regression equation in the range of $C = 0.01$ μg/mL to 5.0 μg/mL was linear ($Y = 0.7871C + 0.0062$, $r = 0.9998$, where Y indicates the area ratio of IBR to the internal standard substance). Pharmacokinetic analyses were conducted using the DAS 2.0 software.

In Vivo Antitumor Activity

The antitumor activities of IBR-PC were investigated using an allograft mouse model of S180 tumors. In brief, tumors were established by injecting S180 cells (1×10^6 cells per mouse) subcutaneously into the right axillary flank of male Kunming mice (26,27). The mice were randomly divided into three groups ($n = 6$ mice per group) and treated *via* intragastric administration of 20 mg/kg IBR-susp and IBR-PC on days 3, 4, 5, 6, 7, 8, 9, 10, 11, and 12. The mice administered with 0.9% normal saline were set as control. The mice were weighed every other day throughout the trial to assess the toxicity of the IBR formulation, and tumor size was measured using an electronic Vernier caliper. Tumor volume was calculated using the formula $V = 0.5 \times (a \times b^2)$, where a and b are the largest and smallest diameters, respectively. Percentage inhibition ratio was calculated as follows: Percentage inhibition ratio (%) = $(V_{Control} - V_{Treated}) / V_{Control} \times 100\%$, where $V_{Control}$ and $V_{Treated}$ are the average tumor volume of the control group and the appropriate treatment group, respectively. Net body weight was calculated using the formula $W_{Net} = W - \rho \times V$, where W is the total mass of mice which includes the mass of tumor, V is the tumor volume, and ρ is tumor the density and it approximated as being equal to that of water.

To objectively evaluate the therapeutic effect of different IBR formulations toward the tumor-bearing mice, we combined two indicators, namely, net body weight and tumor volume. Tumor inhibition (TI) index was calculated to comprehensively evaluate both the antitumor effect and toxicity of the IBR formulations. TI index was calculated as follows:

$$\text{TI index } \left(\text{g/cm}^3\right) = \frac{\text{Net body weight (g)}}{\text{Tumor volume (cm}^3\text{)}}$$

Toxicity Evaluation

The spleen and thymus gland indices (weight of spleen or thymus gland/body weight of mouse, mg/g) were calculated and the histopathological examination was performed to evaluate the toxicity of the different formulations toward the immune organs. On day 17 after tumor inoculation, the mice were sacrificed for tissue harvesting, and the spleens and thymuses were weighed. Then, the tissues were fixed with 4% formaldehyde for 48 h, embedded in paraffin, and cut into slices for histopathology analysis with hematoxylin and eosin (H&E) staining. Finally, the sections were observed by a digital microscope.

Statistical Analysis

Difference between groups was evaluated through unpaired t test by using the ANOVA of SPSS 21.0 software. Data are expressed as mean ± SD and considered statistically significant at $P < 0.05$.

RESULTS AND DISCUSSION

Optimization of Formulation and Processing Parameters

Determine of Formulations

According to the characteristics of the drug and the phospholipid, PC can be prepared through solvent evaporation, freeze-drying, anti-solvent precipitation, supercritical anti-solvent precipitation, and salting-out method. Solvent evaporation is one of the most ubiquitous and simply equipped among these methods. In this study, solvent evaporation is also suitable for IBR fabrication.

The primary consideration prior to preparation is the type of phospholipids to which the IBR can be hydrogen-bonded and the capability of these phospholipids for self-assembly into a PC. Five commonly used phospholipids were selected as candidate excipients; under uniform processing parameters, these phospholipids were dissolved and refluxed together with IBR in a co-solvent. The appearance of the resulting suspensions was examined. The results showed that none of the E80, S100, and DOPA can combine with IBR to form a stable PC, resulting in a white turbid liquid. PS90 also failed to combine with IBR, thereby resulting in a yellow turbid liquid. By contrast, EPG bound easily to IBR and formed a clear solution through self-assembly.

To determine the optimal formulation, we refluxed different molar ratios of IBR and EPG in the co-solution and determined the complexation rate for each formulation. As shown in Fig. 1a, the formulation with the highest complexation rate was obtained when the molar amount of

EPG was the same as that of IBR. With an insufficient amount of EPG, loading of all IBR becomes difficult. Interestingly, an excess of EPG may not increase the complexation rate.

Determination of Processing Parameters

Taking into account the factors that affect the rate of PC formation mainly include solvent type, stoichiometry and concentration of active ingredients, reaction temperature, and reaction time. The complexation rate of the IBR-PC with the same molar ratio but different processing parameters, including reaction time, reaction temperature, and IBR concentration, was recorded.

As the reaction temperature increased from 30to 40°C, the complexation rate of IBR-PC increased considerably (Fig. 1b). Specifically, the complexation rate reached 90.8% ± 5.2% at 40°C; however, further increase in temperature did not result in increase in efficiencies. A similar trend can be observed in Fig. 1c. As the reaction time increased to 0.5 h, the complexation rate gradually increased to 92.0% ± 3.3%. However, no difference in the complexation rate was noted when the reaction time was further increased. These results show that a high complexation rate required sufficient reaction temperature and time, but an excessively high temperature and time no longer exerted effect on complexation rate of PC.

IBR concentration also markedly affected drug loading (Fig. 1d). When IBR concentration was between 5 and 10 mg/mL, the complexation rate was not markedly affected, and these formulations achieved a complexation rate of nearly 90%. However, the complexation rate was substantially reduced when the concentration of IBR in the reaction system further increased. The probable cause for this trend is that the capacity of IBR to come into contact with the EPG in the solvent is insufficient when the concentrations of both materials in the system were excessively high.

Lyophilization of IBR-PC

Lyophilization is a commonly technique used for long-term storage of nanoparticles (28). Three lyoprotectants were added to a solution prior to lyophilization to prevent the PC from coalescing and maintain its nanosize during the process. The appearances of the lyophilized IBR-PC with diverse lyoprotectants (5%, *m*/*v*) are shown in Fig. 2. The freeze-dried PC added with 5% (*m*/*v*) lactose as lyoprotectant resembled a white dense cake, and its mechanical strength cannot be destroyed by slight vibrations. The formulation exhibited a uniform color and was plumb. By contrast, the two other freeze-dried formulations with sucrose and maltose showed a shrinking and inhomogeneous appearance.

With the addition of distilled water and with gentle shaking, lactose-containing formulations can reconstitute the clear solution from the lyophilized powder within seconds (Table I) and its particle size did not significantly change ($P > 0.05$) after reconstitution. By comparison, the formulations with sucrose or maltose as lyoprotectant took longer time to reconstitute as a solution.

On the basis of these results, 5% lactose exhibited further advantage over the two other lyoprotectants in terms of morphological characteristics and reconstruction time of the lyophilized powder; thus, 5% lactose is a good-quality freeze-drying protective agent.

Optimal Formulation and Processing Parameters

According to the above experimental results, the optimal formulation and processing parameters to obtain the best appearance and the highest drug loading are as follows: phospholipid, EPG; molar ratio of IBR and phospholipids, 1:1; IBR concentration, 10 mg mL^{-1}; reaction temperature, 40°C; and reaction time, 30 min. Lactose (5%, *m*/*v*) was added to the IBR-PC as lyoprotectant.

Characterization of IBR-PC

Particle Size, Zeta Potential, and Morphology

Three batches of IBR-PC prepared using the optimal formulation and processing parameters were analyzed in this study. The particle size, PDI, and zeta potential were 29.6 ± 3.4 nm, 0.194 ± 0.021, and 8.02 ± 0.15 mV, respectively.

The morphology of the IBR-PC was determined using TEM (Fig. 3a). The particle size of the complexes as observed under TEM was consistent with the data obtained through dynamic light scattering, and most of the particles are 26–34 nm in size. IBR-PC showed a spherical morphology with a narrow and uniform size distribution in the nanometer range.

Fourier Transform Infrared Spectroscopy

Typical FT-IR spectra were obtained to determine whether a possible interaction occurred between IBR and EPG. As shown in Fig. 3b, the spectrum of the IBR/EPG mixture nearly exhibited an additive effect and includes the characteristic absorption peaks of IBR and EPG. The spectrum contained two stretching vibrations of IBR (3469.3 and 3636.3 cm^{-1}), hydrocarbon stretching vibration of long fatty chain (2921.8 and 2853.4 cm^{-1}), C=O stretching vibration (1256.0 cm^{-1}), and P–O stretching vibration (1115.2 cm^{-1}) of EPG. These results indicated that no interaction occurred between IBR and EPG in the mixtures and that IBR maintained its crystal form.

Contrary to the spectra of the IBR/EPG mixture, the spectrum of IBR-PC slightly changed. First, the double peaks of stretching vibration ($–NH_2$) of IBR disappeared, and only a single peak (3418.0 cm^{-1}) was observed. The intensity of the carbonyl stretching vibration of aliphatic carbonate (1739.1 cm^{-1}) and P–O (1114.6 cm^{-1}) significantly weakened, whereas the intensity and peak position of the carbon-hydrogen stretching vibration of the long fatty chain did not change. Therefore, the interaction between IBR and EPG in the PC was not a simple physical mixing, and long fatty chains were not involved in this interaction. Based on these results, the hydrogen atom on the primary amine group of IBR possibly formed a hydrogen bond with the oxygen atom on aliphatic carbonate or with the phosphorus atom of EPG, although further characterization tests are required.

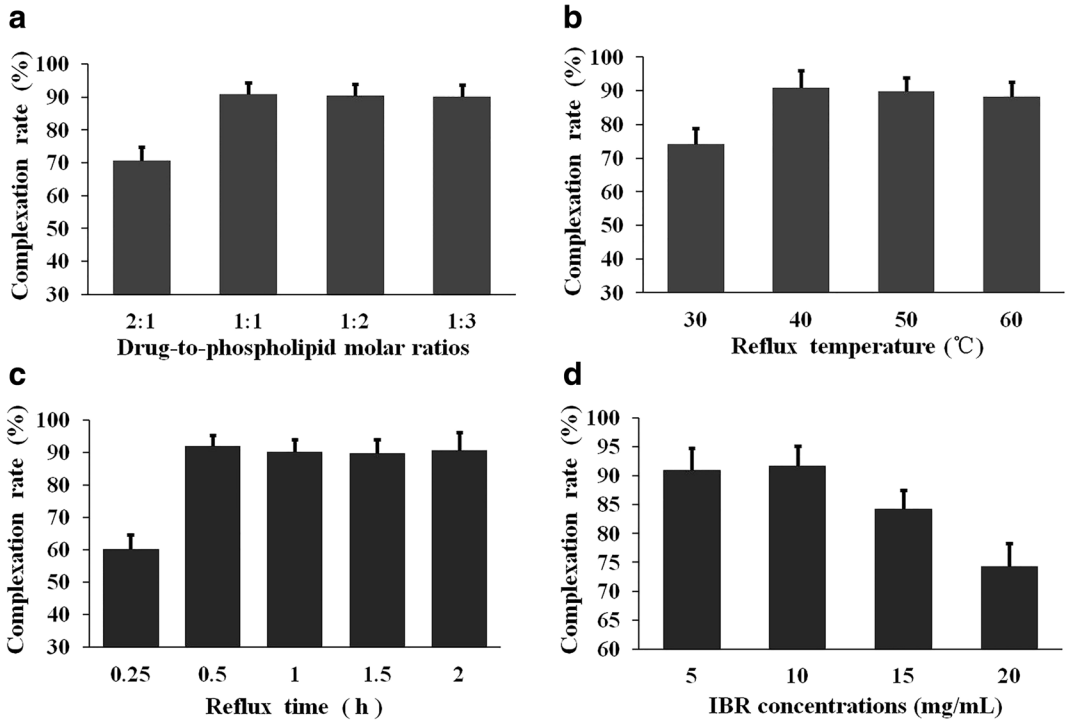

Fig. 1. Complexation rate of IBR-PC at different **a** drug-to-phospholipid molar ratios, **b** reflux temperature, **c** reflux times, and **d** IBR concentrations. Data are presented as mean ± SD, $n = 3$

Differential Scanning Calorimetry

DSC is another common method used in compatibility analysis that provides abundant information on the possible interactions between drugs and excipients (29). Figure 3c shows the DSC thermograms of pure IBR, EPG, IBR/EPG mixture, and IBR-PC. Pure IBR showed an endothermic melting peak at approximately 157°C, and the blank phospholipids showed a melting peak at approximately 87°C. These melting peaks were displayed by the mixture, and no new peaks corresponding to glass transition or recrystallization were observed. However, the melting peak of IBR in the mixture decreased. A possible explanation for this observation is that IBR melts and dissolves in phospholipids as temperature rises, and this phenomenon may partially lead to the formation of complexes. (29,30). For IBR-PC, no endothermic peak was found in IBR, demonstrating that the crystallinity of IBR disappeared due to hydrogen bonding and the van der Waals interactions between the two substances (30,31).

X-ray Powder Diffraction

XRPD was performed to assess the existing form of IBR in PC (Fig. 3d). The XRPD of IBR showed multiple sharp characteristic crystalline peaks at 18.95° and 21.29°, indicating the crystalline characteristics of IBR. The characteristic crystalline signals of IBR were still observed in the diffraction spectrum of its mixture, indicating that IBR in the mixture remained crystalline. However, the characteristic sharp peaks of the drug disappeared in the complex owing to the transformation from crystalline to amorphous state (32,33).

Molecular Docking and Simulation

Molecular docking is a computational procedure that attempts to efficiently predict noncovalent binding of macromolecules or frequently of a macromolecule (receptor) and a small molecule (ligand), starting with their unbound structures, structures obtained from MD simulations, or homology

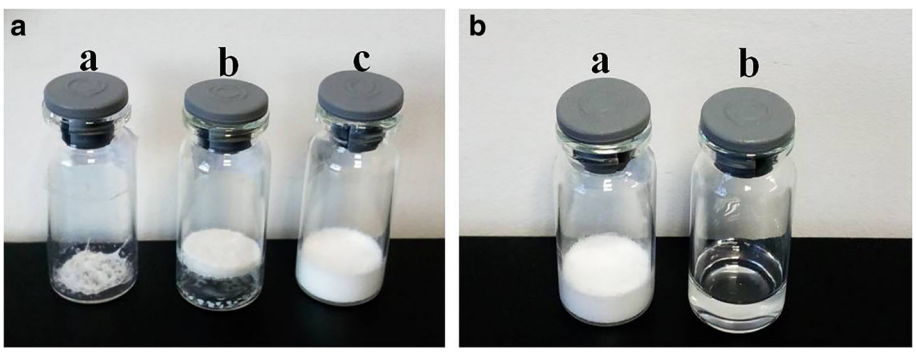

Fig. 2. **a** Appearance of IBR-PC containing a sucrose, b maltose, and c lactose after lyophilization ($n = 3$). **b** Appearance of IBR-PC with lactose after a lyophilization and b reconstitution ($n = 3$)

Table I. Characteristics of Lyophilized IBR-PC with Different Lyoprotectants

Type of lyoprotectant	Sucrose	Maltose	Lactose
Particle size (nm)	31.7 ± 3.4	79.2 ± 8.2	30.7 ± 3.5
Particle size change (nm)	2.1 ± 0.5	49.6 ± 5.3	1.1 ± 0.6
PDI	0.194 ± 0.030	0.326 ± 0.081	0.179 ± 0.025
Reconstitution time (s)	44 ± 7	20 ± 4	12 ± 2

Distilled water was used as reconstitution medium, and the particle size before lyophilization was 29.6 ± 2.9 nm. Data are presented as mean ± SD, $n = 3$. *PDI* polydispersity index

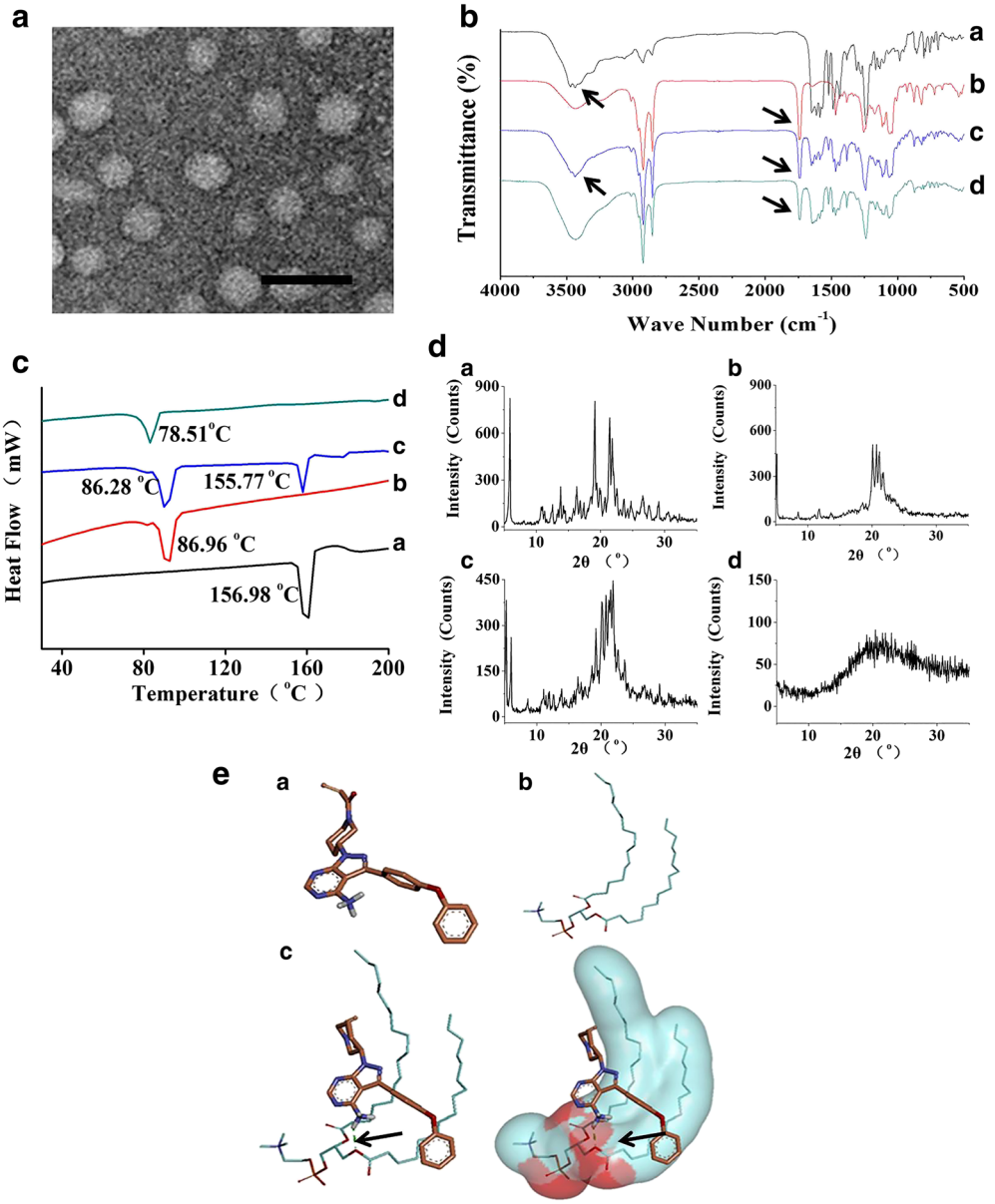

Fig. 3. Characterization of IBR-PC. **a** Transmission electron microscopic image of IBR-PC. Scale bar, 50 nm. **b** IR spectrum of a IBR, b EPG, c IBR/EPG mixture, and d IBR-PC. **c** DSC thermograms of a IBR, b EPG, c IBR/EPG mixture, and d IBR-PC. **d** XRPD spectra of a IBR, b EPG, c IBR/EPG mixture, and d IBR-PC. **e** Molecular docking images depicting the binding of IBR with EPG. a Molecular structure of IBR. b Molecular structure of EPG. c The lowest binding energy conformations of IBR and EPG were obtained through molecular docking calculation. For IBR, orange represents carbon atoms, red represents oxygen, navy blue represents nitrogen, and white represents hydrogen. For EPG, light blue, red, and white represent carbon, oxygen, and hydrogen, respectively; green represents hydrogen bonding

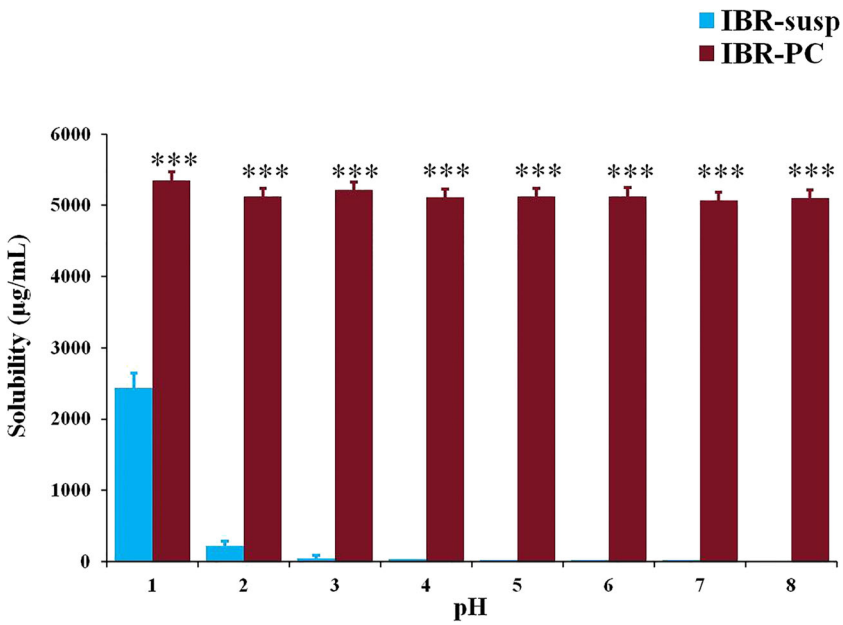

Fig. 4. Solubility of IBR-susp and IBR-PC in media with different pH values. Data are presented as mean ± SD, $n = 3$. ***$P < 0.001$ compared with IBR-susp at the same pH value

modeling. Figure 3e shows the site of interaction between IBR and EPG, wherein the green dashed line represents the hydrogen bonding between terminal primary amine groups of IBR with the carbonyl oxygen on fatty acid esters of EPG. The formation of intermolecular hydrogen-bonding interactions is possibly due to the structural similarity of IBR with EPG in terms of physiochemical properties (34,35).

In summary, IBR can tightly bind to EPG through the hydrogen-bonding interaction.

Solubility Test

Next, the solubility of IBR-susp and IBR-PC in media with different pH values was determined. The results show that the solubility of IBR-susp was markedly affected by pH compared with that of IBR-PC. The solubility of IBR-susp in the medium with a pH of 7 is less than 1/185th of the solubility in the medium with a pH of 1 (Fig. 4). However, IBR-PC can significantly increase the solubility of IBR (exceeded 5 mg/mL) at different pH values ($P < 0.001$). The solubility of IBR-PC in the medium with a pH of 7 (5070.11 ± 112.04 μg/mL) was approximately 380 times that of IBR-susp (13.19 ± 0.21 μg/mL). This markedly improved solubility is related to the amorphous nature of PC. Meanwhile, the crystalline characteristics of IBR were inhibited, so the drug was not required to overcome the lattice when dissolved. As an amphiphilic surfactant, phospholipids that self-assemble in water to form micelles may also serve as solubilizing agent (36).

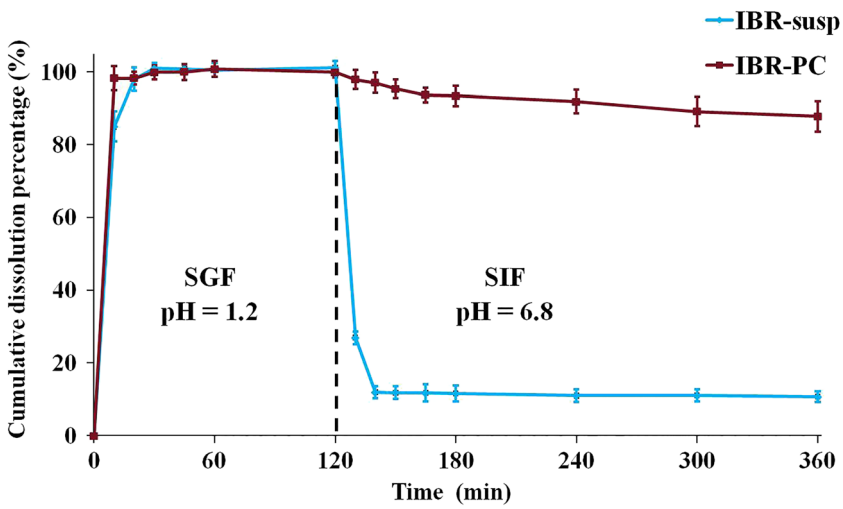

Fig. 5. Dissolution test of IBR-susp and IBR-PC in simulated gastrointestinal fluid. Dissolution profiles of the different formulations were obtained in SGF (pH 1.2) for 2 h and then in SIF (pH 6.8) for 4 h. Data are presented as mean ± SD, $n = 6$. SGF simulated gastric fluid, SIF simulated intestinal fluid

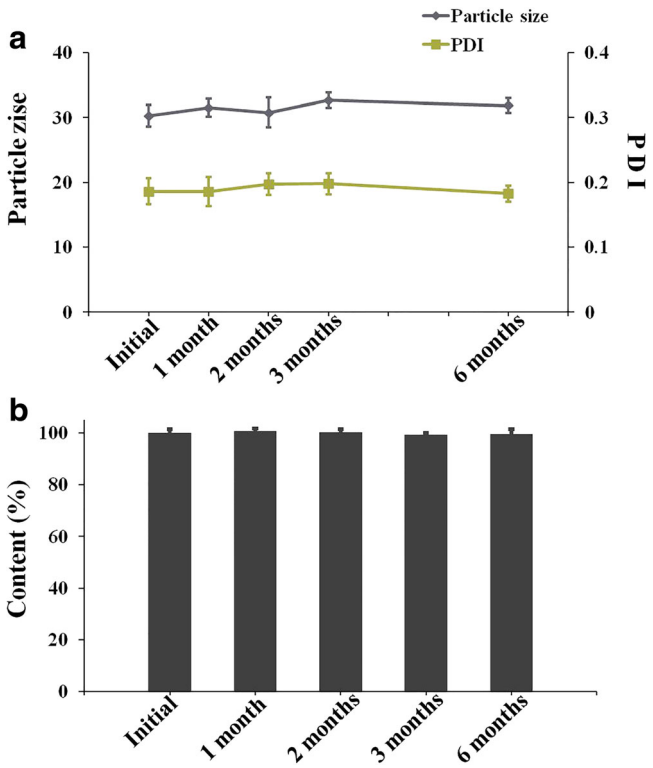

Fig. 6. Changes in **a** particle size, PDI, and **b** drug content of lyophilized IBR-PC. Data are presented as mean ± SD, $n = 3$

In Vitro Dissolution Test in SGIF

To mimic the behavior of the formulation in the gastrointestinal tract, we determined the dissolution of the formulation in SGIF. As shown in Fig. 5, IBR-susp and IBR-PC exhibited a complete dissolution (nearly 100%) in the first 2 h. However, after switching to SIF, the cumulative dissolution percentage of IBR-susp decreased markedly, whereas that of IBR-PC did not show any significant reduction. Specifically, the cumulative dissolution percentage of IBR-susp in SIF was approximately 14%, whereas that of IBR-PC remained above 85% throughout the experiment. When the IBR was transported and moved from the stomach to the intestine, its solubility substantially decreased as the pH increased, possibly leading to precipitation of large amounts of drugs in the intestinal tract. This phenomenon may induce a series of severe gastrointestinal side effects, including diarrhea and nausea (37).

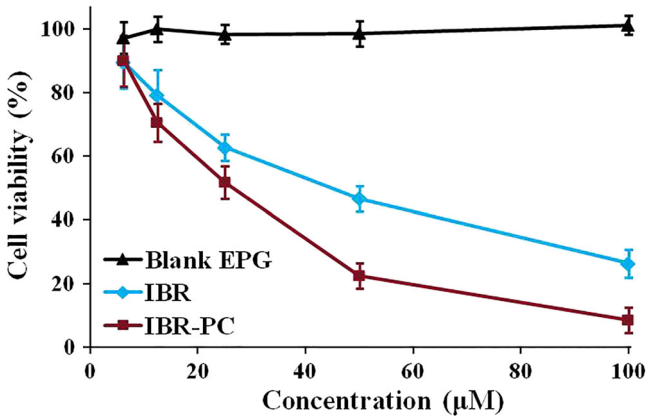

Fig. 7. Cell cytotoxicity of blank EPG, IBR, and IBR-PC on S180 cells. Data are presented as mean ± SD, $n = 3$

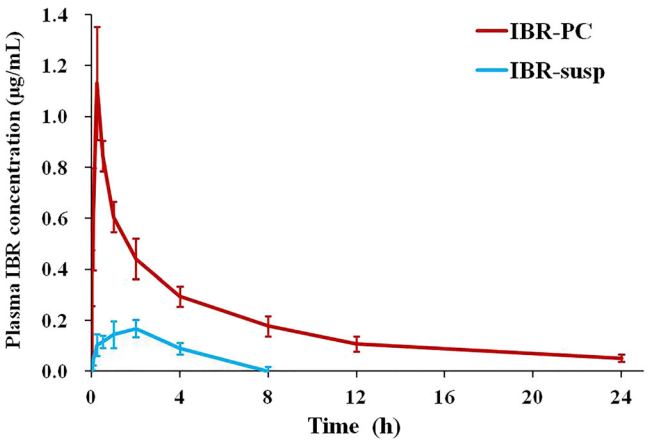

Fig. 8. Plasma concentration of IBR in Wistar rats after intragastric administration of different IBR formulations. Data are presented as mean ± SD, $n = 3$

For the IBR-PC formulation, dissolution slightly decreased with the increased mixing time. This observation may be attributed to a small amount of drug that leaked from the carrier into the medium and then precipitated after switching to SIF. However, the vast majority of IBR can form tight linkage with phospholipids through hydrogen bonding in SGIF, confirming that the formulation can maintain a high degree of stability in the gastrointestinal tract. This stability further promotes drug absorption and reduces the side effects in the gastrointestinal tract.

Long-term Stability of Lyophilized IBR-PC

To determine the physical and chemical stability of the lyophilized IBR-PC, we monitored the particle size and content after 0, 1, 2, 3, and 6 months of storage at 4°C ± 2°C. When reconstituted with distilled water, the formulation remained colorless, clear, and transparent. No significant changes in terms of concentration and particle size were observed in any formulation after long-term storage (Fig. 6, $P > 0.05$).

MTT Assay

The *in vitro* cytotoxicity of the different formulations was evaluated in S180 cells (Fig. 7). For the IBR

Table II. Major Pharmacokinetic Parameters of IBR-PC and IBR-Susp in Wistar Rats

Parameters	IBR-susp	IBR-PC
C_{max} (μg/mL)	0.180 ± 0.079	1.13 ± 0.221**
T_{max} (h)	1.333 ± 0.577	0.25*
$AUC_{(0-t)}$ (μg/mL h)	0.496 ± 0.301	4.534 ± 1.618*

Data are presented as mean ± SD, $n = 3$. *$P < 0.05$, **$P < 0.01$ compared with IBR-susp. *IBR-susp* IBR suspension, *IBR-PC* ibrutinib-phospholipid complex, C_{max} maximum plasma concentration, T_{max} maximum time, $AUC_{(0-t)}$ area under concentration

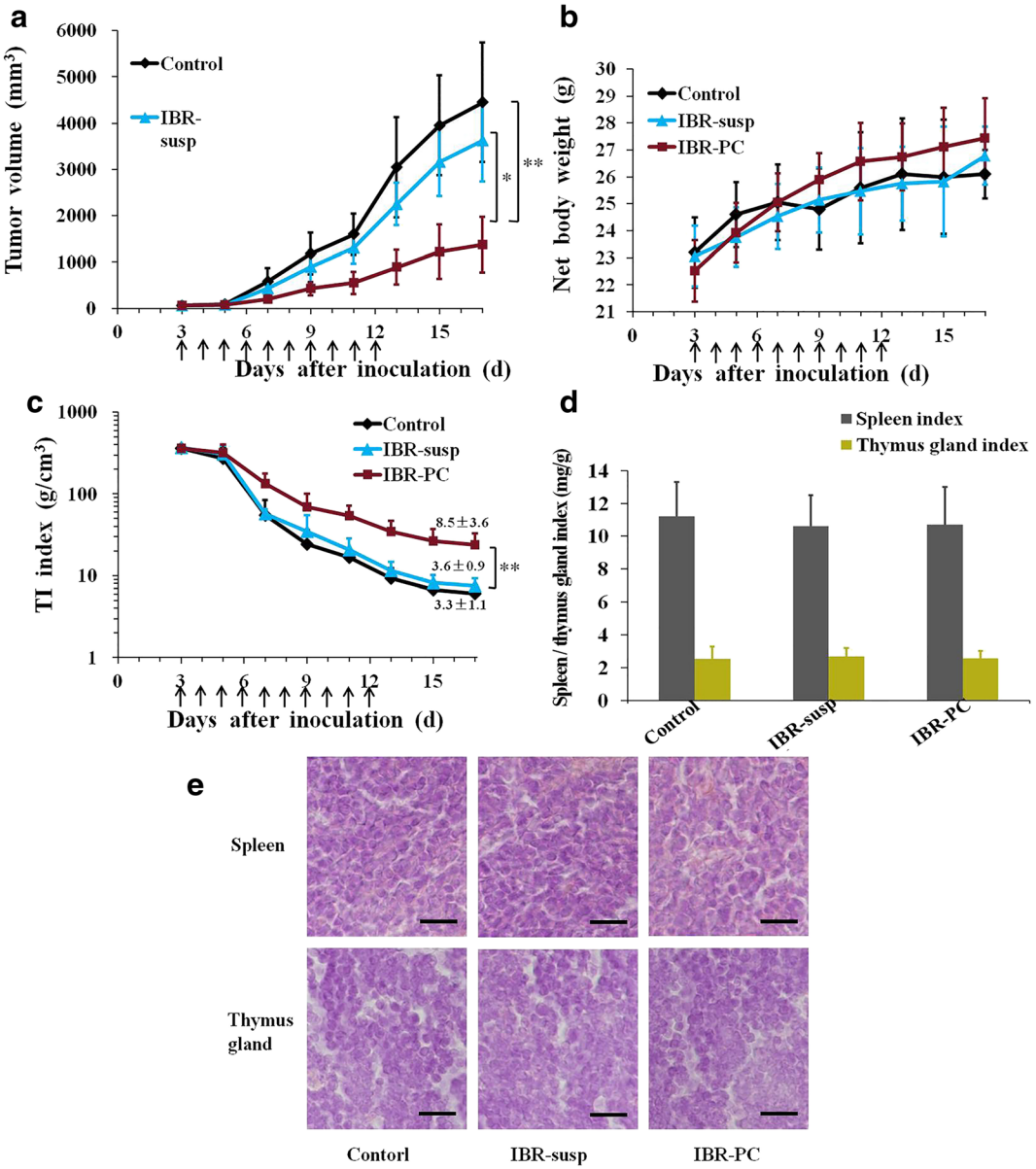

Fig. 9. **a** Tumor growth curve, **b** net body weight change, **c** TI index, and **d** spleen and thymus gland indices of tumor-bearing mice administered with different formulations. Data are presented as mean ± SD, $n = 5$ to 6. $^{*}P < 0.05$, $^{**}P < 0.01$ compared with the control group. TI index tumor inhibition index. **e** Histopathology of spleen and thymus gland with hematoxylin and eosin (H&E) staining of different experimental groups. Scale bar, 100 μm

formulations, the inhibitory ratios of S180 cells represented to be dose-dependent. The IC_{50} value of IBR-PC (26.09 ± 2.30 μM) was also found significantly lower than free IBR (43.48 ± 4.12 μM, $P < 0.01$). In contrast, blank EPG elucidated no cytotoxicity against the tumor cells, reserving its non-toxic excipient status. Thus, these results revealed that IBR-PC displayed higher cytotoxicity to S180 cells as compared to free drugs.

Pharmacokinetic Studies

Improved oral bioavailability is a key determinant for the further application of a drug in clinical setting. Therefore, the pharmacokinetic characteristics of IBR-susp and IBR-PC were evaluated in rats. The corresponding plasma IBR concentration curves after oral administration of IBR-susp and IBR-PC are shown in Fig. 8, and the corresponding pharmacokinetic parameters are shown in Table II.

According to the drug-time curve, the rats showed the maximum plasma concentration (0.180 ± 0.079 μg/mL) at 1.33 h after oral administration of IBR-susp. By contrast, the rats showed a significantly higher maximum plasma concentration (1.130 ± 0.221 μg/mL) at 0.25 h after oral administration of IBR-PC ($P < 0.01$). The $AUC_{(0–24\ h)}$ for the IBR-PC group was a 9.14-fold improvement relative to that for the IBR-susp group. IBR cannot be completely dissolved in the finite volume of the oral solution, and this observation is possibly responsible for the adverse effect of the absorption of the IBR in the

gastrointestinal tract and the low drug bioavailability. Moreover, the IBR-PC group showed a reduced t_{max} compared with the IBR-susp group. This result indicated the faster onset of action owing to the significantly improved rate of drug absorption from the prepared formulations.

The promotion of the relative bioavailability of IBR after oral administration can be explained as follows:

(1) The hydrophilicity of poorly soluble IBR were considerably enhanced due to the interaction with miscible EPG through hydrogen bonding and subsequent self-assembly to form vehicles (36). Moreover, IBR is distributed in the complex in an amorphous state, resulting in elevated solubility and increased dissolution rate (38).
(2) IBR-PC can easily penetrate the cell membrane and enter the cytoplasm of living mammalian cells, and this phenomenon is ascribed to the fact that phospholipids are an important component of cell membranes and display a good biocompatibility (39). In addition, the nanosize of IBR-PC may increase oral absorption *via* the Peyer's patches and M cells in the intestine (40,41).

In short, the results illustrated that the bioavailability of IBR-PC substantially increased, thereby facilitating the enhancement of the clinical efficacy of the drug.

In Vivo Antitumor Activity

Pharmacokinetic test demonstrated that IBR-PC can maintain a high plasma concentration for extended periods; this characteristic is the key to ensure the efficacy of the drug. Next, the *in vivo* antitumor activity of different IBR formulations was investigated (Fig. 9).

Tumor growth progression clearly demonstrated that the IBR-PC group substantially suppressed tumor growth compared with the control group (Fig. 9a, $P < 0.01$). Tumor volume was markedly restrained after several treatments with IBR-PC and percentage inhibition ratio was $69.5\% \pm 13.4\%$. Moreover, the antitumor efficacy of IBR-PC was significantly superior to that of IBR-susp group ($P < 0.05$), and the percentage inhibition ratio of IBR-PC group was more than three times that of the IBR-susp group. The improved bioavailability of IBR-PC results in a large amount of drug entering the circulatory system; this phenomenon may explain the higher inhibitory effect of IBR-PC than that of the IBR-susp.

The ultimate goal of cancer therapy is to increase the survival time and improve the quality of life of patients by reducing the systemic toxicity of chemotherapy (42). Thus, the body mass of all mice in each group was recorded and the net body weight was calculated (Fig. 9b). During the experimental period, the net body weight of mice in different groups increased steadily, and no significant discrepancy between groups was noted ($P > 0.05$), demonstrating that IBR does not exert a severe systemic toxicity. Given that there was no significant difference in the net weight of mice in each group, TI index was quoted to comprehensively appraise the efficacy of the formulation (Fig. 9c) (43). TI index of IBR-PC (23.7 ± 9.3 g/cm^3) on day 17 was considerably higher than that of the two other groups ($P < 0.01$), indicating a secure and efficient antitumor efficacy.

Given that numerous other targets of IBR are expressed in immune cells (44,45), further evaluation of damage in immune organs is necessary. Thus, spleen and thymus gland indices were calendared to characterize the toxicity induced by different IBR formulations (46,47). The result shows that the spleen and thymus indices did not significantly differ between groups (Fig. 9d, $P > 0.05$), demonstrating that the IBR-PC formulation exhibits low systemic toxicity. Moreover, consistent results can be observed from pathological examination of immune organs (Fig. 9e).

The results of this study suggest that IBR-PC shows higher tumor growth suppression compared with the suspension, while showing no additional systemic toxicity and tissue side effects.

CONCLUSIONS

Most researches have used soy lecithin as an excipient to prepare PC, and EPG has not been reported. In this work, a stable IBR-PC complex was successfully fabricated using EPG as adjunct for the first time. The complex was assessed by TEM, FT-IR, DSC, XRD, and molecular docking and simulation studies. No chemical degradation or change in particle size of IBR-PC was observed during the 6-month storage. Compared with the solubility of IBR-susp, that of the IBR-PC is significantly increased at different pH values. *In vitro* dissolution test demonstrated that compared with the suspension, IBR-PC displays better dissolution profiles and higher gastrointestinal stability, leading to a significant increase in oral bioavailability. Moreover, *in vitro* cytotoxicity studies and *in vivo* antitumor efficacy of IBR-PC in tumor-bearing mice illustrated that IBR-PC displayed superior growth inhibition of tumor cells. Therefore, the development of IBR-PC is a promising approach to improve the oral bioavailability and reduce the toxicity of IBR.

ACKNOWLEDGEMENTS

This research was supported by the National Natural Science Foundation of China (No. 81373334 and No. 81573375).

COMPLIANCE WITH ETHICAL STANDARDS

All animal experiments were performed in accordance with the guidelines of the Animal Welfare Committee of Shenyang Pharmaceutical University. The protocol numbers of the animal studies were SYPU-IACUC-C2018-1-24-201 and SYPU-IACUC- C2018-4-4-101.

Conflict of Interest The authors declare that they have no conflict of interest.

REFERENCES

1. Woyach JA, Johnson AJ, Byrd JC. The B-cell receptor signaling pathway as a therapeutic target in CLL. Blood. 2012;120(6):1175–84.
2. Rauf F, Festa F, Park JG, Magee M, Eaton S, Rinaldi C, et al. Ibrutinib inhibition of ERBB4 reduces cell growth in a WNT5A-dependent manner. Oncogene. 2018;37(17):2237–50.
3. Advani RH, Buggy JJ, Sharman JP, Smith SM, Boyd TE, Grant B, et al. Bruton tyrosine kinase inhibitor ibrutinib (PCI-32765) has significant activity in patients with relapsed/refractory B-cell malignancies. J Clin Oncol. 2012;31(1):88–94.
4. Barrientos J, Rai K. Ibrutinib: a novel Bruton's tyrosine kinase inhibitor with outstanding responses in patients with chronic lymphocytic leukemia. Leuk Lymphoma. 2013;54(8):1817–20.
5. Nalley C. Ibrutinib granted breakthrough therapy designation by FDA for cGVHD treatment. Oncology Times. 2016;38(14):5–6.
6. Honigberg LA, Smith AM, Sirisawad M, Verner E, Loury D, Chang B, et al. The Bruton tyrosine kinase inhibitor PCI-32765 blocks B-cell activation and is efficacious in models of autoimmune disease and B-cell malignancy. Proc Natl Acad Sci. 2010;107(29):13075–80.
7. Berglöf A, Hamasy A, Meinke S, Palma M, Krstic A, Månsson R, et al. Targets for ibrutinib beyond B cell malignancies. Scand J Immunol. 2015;82(3):208–17.
8. Wang X, Wong J, Sevinsky CJ, Kokabee L, Khan F, Sun Y, *et al.* Bruton's tyrosine kinase inhibitors prevent therapeutic escape in breast cancer cells. Molecular cancer therapeutics. 2016:molcanther. 0813.2015.
9. Cohen MS, Zhang C, Shokat KM, Taunton J. Structural bioinformatics-based design of selective, irreversible kinase inhibitors. Science. 2005;308(5726):1318–21.
10. Leproult E, Barluenga S, Moras D, Wurtz J-M, Winssinger N. Cysteine mapping in conformationally distinct kinase nucleotide binding sites: application to the design of selective covalent inhibitors. J Med Chem. 2011;54(5):1347–55.
11. Use CfMPfH. Guideline on the investigation of bioequivalence. London: European Medicines Agency; 2010.
12. Zvonicek V, Skorepova E, Dusek M, Babor M, Zvatora P, Soos M. First crystal structures of pharmaceutical ibrutinib: systematic solvate screening and characterization. Cryst Growth Des. 2017;17(6):3116–27.
13. de Jésus NP, Kabamba B, Dahlqvist G, Sempoux C, Lanthier N, Shindano T, et al. Occult HBV reactivation induced by ibrutinib treatment: a case report. Acta Gastro-Enterol Belg. 2015;78
14. Atluri H, Chong CW, Kuehl R, Shu C, Tay PS-C, Hulvat JF, *et al.* Novel formulations of a Bruton's tyrosine kinase inhibitor. Google Patents; 2017.
15. Chen M, Zhang Y, Chaohui Y, Zhang X, Wang P, Li P, *et al.* Crystalline form I of ibrutinib. Google Patents; 2017.
16. Sebastian R, Erdmann M, Albrecht W. Acid addition salt of ibrutinib. Google Patents; 2017.
17. Shakeel F, Iqbal M, Ezzeldin E. Bioavailability enhancement and pharmacokinetic profile of an anticancer drug ibrutinib by self-nanoemulsifying drug delivery system. J Pharm Pharmacol. 2016;68(6):772–80.
18. Mukherjee P, Maiti K, Kumar V. Value added drug delivery systems with botanicals: approach for dosage development from natural resources. Pharm Rev. 2007;6:57–60.
19. Samuni A, Chong PL, Barenholz Y, Thompson T. Physical and chemical modifications of adriamycin: iron complex by phospholipid bilayers. Cancer Res. 1986;46(2):594–9.
20. Tanhuanpää K, Cheng KH, Anttonen K, Virtanen JA, Somerharju P. Characteristics of pyrene phospholipid/γ-cyclodextrin complex. Biophys J. 2001;81(3):1501–10.
21. Raju TP, Reddy MS, Reddy VP. Phytosomes: a novel phyto-phospholipid carrier for herbal drug delivery. Int Res J Pharm. 2011;2(6):28–33.
22. Loguercio C, Andreone P, Brisc C, Brisc MC, Bugianesi E, Chiaramonte M, et al. Silybin combined with phosphatidylcholine and vitamin E in patients with nonalcoholic fatty liver disease: a randomized controlled trial. Free Radic Biol Med. 2012;52(9):1658–65.
23. Semalty A, Semalty M, Rawat B, Singh D, Rawat M. Pharmacosomes: the lipid-based new drug delivery system. Expert Opin Drug Deliv. 2009;6(6):599–612.
24. Lu M, Qiu Q, Luo X, Liu X, Sun J, Wang C, et al. Phyto-phospholipid complexes (phytosomes): a novel strategy to improve the bioavailability of active constituents. Asian J Pharm Sci. 2018. https://doi.org/10.1016/j.ajps.2018.05.011.
25. Trott O, Olson AJ. AutoDock Vina: improving the speed and accuracy of docking with a new scoring function, efficient optimization, and multithreading. J Comput Chem. 2010;31(2):455–61.
26. Zhou S, Zhang T, Peng B, Luo X, Liu X, Hu L, et al. Targeted delivery of epirubicin to tumor-associated macrophages by sialic acid-cholesterol conjugate modified liposomes with improved antitumor activity. Int J Pharm. 2017;523(1):203–16.
27. Shi J, Zhou S, Kang L, Ling H, Chen J, Duan L, et al. Evaluation of the antitumor effects of vitamin K2 (menaquinone-7) nanoemulsions modified with sialic acid-cholesterol conjugate. Drug Deliv Transl Res. 2018;8(1):1–11.
28. Abdelwahed W, Degobert G, Stainmesse S, Fessi H. Freeze-drying of nanoparticles: formulation, process and storage considerations. Adv Drug Deliv Rev. 2006;58(15):1688–713.
29. Jiang Q, Yang X, Du P, Zhang H, Zhang T. Dual strategies to improve oral bioavailability of oleanolic acid: enhancing water-solubility, permeability and inhibiting cytochrome P450 isozymes. Eur J Pharm Biopharm. 2016;99:65–72.
30. Maiti K, Mukherjee K, Gantait A, Saha BP, Mukherjee PK. Curcumin–phospholipid complex: preparation, therapeutic evaluation and pharmacokinetic study in rats. Int J Pharm. 2007;330(1–2):155–63.
31. Jena SK, Singh C, Dora CP, Suresh S. Development of tamoxifen-phospholipid complex: novel approach for improving solubility and bioavailability. Int J Pharm. 2014;473(1–2):1–9.
32. Zhang Z, Chen Y, Deng J, Jia X, Zhou J, Lv H. Solid dispersion of berberine–phospholipid complex/TPGS 1000/SiO2: preparation, characterization and in vivo studies. Int J Pharm. 2014;465(1–2):306–16.
33. Singh C, Bhatt TD, Gill MS, Suresh S. Novel rifampicin–phospholipid complex for tubercular therapy: synthesis, physicochemical characterization and in-vivo evaluation. Int J Pharm. 2014;460(1–2):220–7.
34. Roderick SL, Chan WW, Agate DS, Olsen LR, Vetting MW, Rajashankar K, et al. Structure of human phosphatidylcholine transfer protein in complex with its ligand. Nat Struct Mol Biol. 2002;9(7):507.
35. Beg S, Raza K, Kumar R, Chadha R, Katare O, Singh B. Improved intestinal lymphatic drug targeting via phospholipid complex-loaded nanolipospheres of rosuvastatin calcium. RSC Adv. 2016;6(10):8173–87.
36. Khan J, Alexander A, Saraf S, Saraf S. Recent advances and future prospects of phyto-phospholipid complexation technique for improving pharmacokinetic profile of plant actives. J Control Release. 2013;168(1):50–60.
37. O'Brien S, Furman RR, Coutre SE, Sharman JP, Burger JA, Blum KA, et al. Ibrutinib as initial therapy for elderly patients with chronic lymphocytic leukaemia or small lymphocytic lymphoma: an open-label, multicentre, phase 1b/2 trial. Lancet Oncol. 2014;15(1):48–58.
38. Tan Q, Liu S, Chen X, Wu M, Wang H, Yin H, et al. Design and evaluation of a novel evodiamine-phospholipid complex for improved oral bioavailability. AAPS PharmSciTech. 2012;13(2):534–47.
39. Awasthi R, Kulkarni G, Pawar VK. Phytosomes: an approach to increase the bioavailability of plant extracts. Int J Pharm Pharm Sci. 2011;3(2):1–3.
40. Peng Q, Zhang Z-R, Sun X, Zuo J, Zhao D, Gong T. Mechanisms of phospholipid complex loaded nanoparticles

enhancing the oral bioavailability. Mol Pharm. 2010;7(2):565–75.
41. Cui F, Shi K, Zhang L, Tao A, Kawashima Y. Biodegradable nanoparticles loaded with insulin–phospholipid complex for oral delivery: preparation, in vitro characterization and in vivo evaluation. J Control Release. 2006;114(2):242–50.
42. Byrne JD, Betancourt T, Brannon-Peppas L. Active targeting schemes for nanoparticle systems in cancer therapeutics. Adv Drug Deliv Rev. 2008;60(15):1615–26.
43. Luo X, Hu L, Zheng H, Liu M, Liu X, Li C, *et al*. Neutrophil-mediated delivery of pixantrone-loaded liposomes decorated with poly (sialic acid)–octadecylamine conjugate for lung cancer treatment.
44. Moreau T, Barlogis V, Bardin F, Nunes J, Calmels B, Chabannon C, et al. Development of an enhanced B-specific lentiviral vector expressing BTK: a tool for gene therapy of XLA. Gene Ther. 2008;15(12):942–52.
45. Hendriks RW, Yuvaraj S, Kil LP. Targeting Bruton's tyrosine kinase in B cell malignancies. Nat Rev Cancer. 2014;14(4):219–32.
46. Cui H, Li T, Wang L, Su Y, Xian CJ. Dioscorea bulbifera polysaccharide and cyclophosphamide combination enhances anti-cervical cancer effect and attenuates immunosuppression and oxidative stress in mice. Sci Rep. 2016;6:19185.
47. Yu F, Yu F, McGuire P, Li R, Wang R. Effects of Hydrocotyle sibthorpioides extract on transplanted tumors and immune function in mice. Phytomedicine. 2007;14(2–3):166–71.